

Distillation of Diffusion Features for Semantic Correspondence

Frank Fundel

Johannes Schusterbauer

Vincent Tao Hu

Björn Ommer

CompVis@LMU Munich, MCML

<https://compvis.github.io/distilldift>

Abstract

Semantic correspondence, the task of determining relationships between different parts of images, underpins various applications including 3D reconstruction, image-to-image translation, object tracking, and visual place recognition. Recent studies have begun to explore representations learned in large generative image models for semantic correspondence, demonstrating promising results. Building on this progress, current state-of-the-art methods rely on combining multiple large models, resulting in high computational demands and reduced efficiency. In this work, we address this challenge by proposing a more computationally efficient approach. We propose a novel knowledge distillation technique to overcome the problem of reduced efficiency. We show how to use two large vision foundation models and distill the capabilities of these complementary models into one smaller model that maintains high accuracy at reduced computational cost. Furthermore, we demonstrate that by incorporating 3D data, we are able to further improve performance, without the need for human-annotated correspondences. Overall, our empirical results demonstrate that our distilled model with 3D data augmentation achieves performance superior to current state-of-the-art methods while significantly reducing computational load and enhancing practicality for real-world applications, such as semantic video correspondence. Our code and weights are publicly available on our project page.

1. Introduction

Semantic correspondence involves finding relationships between different regions across two images, enabling a wide range of applications such as 3D reconstruction [47], image-to-image translation [91], object tracking [22], video segmentation [95], pose estimation [37, 85], explainable AI [87] and visual place recognition [42]. Traditional approaches often rely on handcrafted features like SIFT [58] and SURF [5], which, despite their robustness, have limitations in capturing semantic meaning. With the advent of deep learning, Convolutional Neural Networks [31, 67, 73,

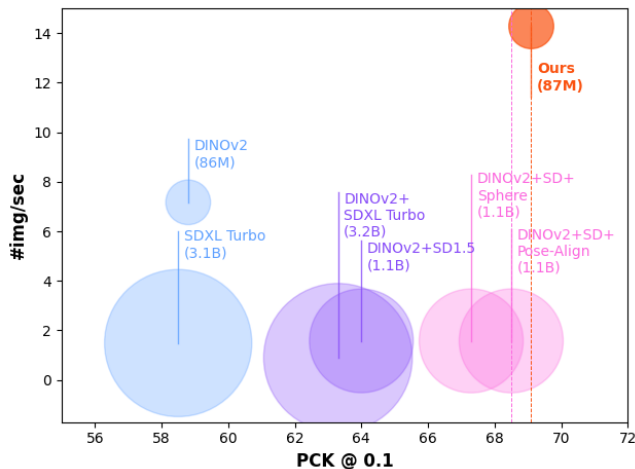


Figure 1. **Our method achieves better performance and throughput with less parameters on the SPair-71k dataset.** The circle size represents number of parameters. For more details, see Tab. 1.

101] and Vision Transformers [11, 12, 40, 43, 45] have revolutionized the field, providing powerful methods to extract semantically rich features from images in various ways. Since finding semantic correspondences is challenging due to the need for extensive world knowledge, the transition to large-scale supervised deep learning was hindered by the limited availability of ground-truth annotations. To address this issue, recent efforts have focused on weakly-supervised [94] and self-supervised methods to extract per-pixel descriptors, most notably DINO [1, 29]. Diffusion Models (DMs) have shown great capabilities in generating high-quality images, due to their large-scale training paradigm which has also led them to learn rich world representations, useful for downstream tasks such as semantic correspondence [32, 90].

Since a previous work “A Tale of Two Features” [102] demonstrated that those two models are complementary in their features, current state-of-the-art approaches [63, 103] all rely on combining two large vision foundation models. This comes with several limitations. First, diffusion mod-

els often need to be run multiple times to incorporate different timesteps, leading to increased computational complexity and longer inference times. Second, these combined models are typically very large networks with a substantial number of parameters, which require significant computational resources and memory. Third, managing these combined models introduces numerous additional hyperparameters, such as timestep(s), layer(s) and prompt, and mixing weights, complicating further training. This becomes particularly challenging when calculating correspondences in videos or in other real-time applications such as semantic video correspondence. Additionally, the increased number of parameters reduces computational efficiency, posing challenges for server-less applications.

Distillation [34] is a well-known method broadly applied in various tasks like classification [55], segmentation [60], self-supervised learning [25] and generative models’ sampling acceleration [78]. This naturally raises a question: can we also apply distillation on top of the ”Tale of Two Features” [102], and ideally squeeze the parameter burden further to boost inference speed in the task of semantic correspondence?

We propose to leverage knowledge distillation for semantic correspondence to reduce the computational load of existing off-the-shelf methods, without retraining a full model. In summary, we make the following contributions:

- We propose a parameter-efficient approach to distill the semantic correspondence capabilities of two complementary large vision foundation models into a more compact and efficient model.
- We additionally propose a novel fine-tuning protocol to further boost the model’s performance by incorporating 3D data augmentation. This approach not only achieves new state-of-the-art results but also allows the model to improve without the need for labeled data.
- We validate the effectiveness of our method on three canonical benchmark datasets, demonstrating state-of-the-art performance on semantic correspondence with significantly reduced inference time.

2. Related Work

Visual Correspondence. Visual correspondence refers to the identification of meaningful associations between different points or regions in images. Traditional methods for geometric correspondence, such as SIFT [58, 59] and SURF [5], involve extracting hand-crafted visual descriptors and matching them across images. Later, it was discovered, that semantic correspondence also emerges in deep Convolutional Neural Network (CNN) features [23, 61, 101, 105] trained on other tasks such as classification. Subsequently, specifically designed

architectures and algorithms were proposed to tackle the task of semantic correspondence using deep features of CNNs [14, 43–45, 48, 49, 51, 56, 74, 75] and recently also transformers [11, 12, 40]. However, finding semantic correspondences is a much more challenging task that requires vast knowledge about the world. Thus, the transition to large-scale supervised deep learning has been impeded by the limited availability of ground-truth correspondence annotations. As a solution to this issue, recent efforts have emerged in the form of weakly-supervised [94] and self-supervised [38] methods to generate per-pixel (dense) descriptors, most notably DINO [1, 29]. DINO is a large Vision Transformer (ViT) [18] trained using a self-distillation approach, where the model learns to predict its own output under different augmentations, effectively leveraging large amounts of unlabeled data to generate high-quality dense descriptors. Generative models need to possess extensive knowledge about the world to synthesize new data accurately. Therefore, the internal representations of large generative models, such as Generative Adversarial Networks (GANs) [24], can be effectively utilized for identifying visual correspondences within specific image categories [68]. Similarly, internal representations of Diffusion Models (DMs) recently demonstrated their potential in various downstream tasks.

Diffusion Model Representations. Diffusion Models have significantly advanced the field of image generation, achieving state-of-the-art performance [17, 76, 82] and their applications extend beyond image creation to various vision tasks such as image segmentation [2, 4, 10, 39, 88, 89, 96], object detection [9], image classification [50, 69], image editing [13, 15, 36, 41, 84] and monocular depth estimation [19, 28, 81, 83]. Recently, there has been a growing interest in exploring the underlying representations of these models, particularly in how they can be leveraged for various downstream tasks [20]. Specifically, several works have demonstrated that the intermediate cross-attention maps of a pre-trained diffusion model can be used for text-based image editing [33, 92], zero-shot segmentation [4, 97, 98] and depth estimation [104]. These methods work by aggregating intermediate feature maps, self- or cross-attention maps from a hand-selected subset of layers and timesteps during the forward diffusion process.

Diffusion Models for Semantic Correspondence. While the applicability of diffusion model representations in various computer vision tasks has been well-established, their use in the domain of semantic correspondence is still an emerging area of research with only a few recent works. Hedlin et al. and Li et al. [32, 54] focus on optimizing the Diffusion Model’s prompt embeddings to find correspondences across images. However, due

to the test-time optimization of the prompt embedding and iterative sampling of the diffusion model, the overall computational efficiency hinders it from being applied to further tasks, such as fine-tuning. Tang et al. [90] present a straightforward approach that utilizes cosine similarity of the intermediate features of two images at a specific timestep and layer to find correspondences using nearest neighbor lookup. Luo et al. [62] introduce a technique that leverages a learned feature aggregation network for combining features over multiple layers and timesteps. “A Tale of Two Features” [102] demonstrate that the features of a Diffusion Model and those of DINOv2 complement each other and that their combined performance is greater than their individual. Additionally, recent studies focus on overcoming the issue of left-right ambiguity [63, 103]. However, while all these methods provide accurate semantic representations, they still rely on aggregating the extracted features of two large vision foundation models, resulting in high computational demands and reduced efficiency.

Knowledge Distillation. Knowledge Distillation is a process where knowledge is transferred from one model, that is typically larger and more complex, to another model, that is usually smaller and more efficient [34]. It has been successfully applied to (large) language models [27, 79], speech recognition models [21] and even diffusion models [26, 64, 78, 83, 86] in various ways. There are three kinds of knowledge: response based [34, 65] (the output layer’s logits), feature based [6, 77, 100] (the intermediate feature maps) and relation based [99] (the relationships between different layers or data samples). Different techniques can be utilized to perform distillation e.g. multi-teacher distillation [71, 80], where multiple teacher models are combined to train a single student model. Pseudo-labeling for distillation [46] involves the generation of pseudo-labels for previously unlabeled data by the teacher model. Some works use cross-entropy between the teacher and student outputs [34, 79]. Others aim to minimize the reverse KLD, which measures how two probability distributions differ [21, 27]. For Diffusion Models, knowledge distillation is primarily applied to reduce the number of diffusion steps needed to generate high-fidelity images, with multiple works utilizing a weighted MSE as the objective [26, 64, 78, 86]. One work [52] specifically focuses on leveraging distillation for semantic correspondence. However, they aim to distill knowledge from a probabilistic model which mimics a group of models into a single static one, whereas our goal is to efficiently distill the knowledge of multiple foundation model teachers into a single smaller model. Furthermore, they utilize synthetic image pairs by augmenting a single image, whereas we make use of real image pairs from a multi-view image dataset. We utilize multi-teacher distillation to distill

the semantic correspondence capabilities of two large models into a single model, by aligning their predicted similarity distributions.

3. Method

Problem Formulation. Semantic correspondence can be defined as follows. For a given pair of images I_1, I_2 and a query keypoint $p_1 \in I_1$, we want to find the corresponding target point $p_2 \in I_2$ with the highest semantic similarity i.e. points of different objects that share semantic meaning. By extracting feature maps $\mathcal{F}_1, \mathcal{F}_2$ from both images, a corresponding target point for p_2 can be obtained with:

$$p_2 = \arg \min_p d(\mathcal{F}_1(p_1), \mathcal{F}_2(p)), \quad (1)$$

where the distance metric $d(\cdot, \cdot)$ is defined as cosine similarity $\text{sim}(\cdot, \cdot)$. Current state-of-the-art methods [63, 102, 103] rely on combining two large vision foundation models, specifically a Vision Transformer and a Diffusion Model. This introduces numerous hyperparameters (e.g., timesteps, layers, prompts, mixing weights), increasing the complexity, and number of parameters. As a result, fine-tuning is difficult, VRAM requirements are higher, and computational efficiency is reduced, challenging server-less or real-time deployment. In this work, we address these issues by distilling information from these two large vision foundation models into a single model. This approach significantly reduces complexity and decreases the number of parameters, thereby improving efficiency without compromising performance. Furthermore, we show that by incorporating 3D data from a multi-view image dataset, we can fine-tune our model without the expense of human-annotated data.

3.1. Preliminaries

We leverage two major models that have shown strong performance in semantic correspondence: Stable Diffusion [76] is a text-conditioned Latent Diffusion Model (LDM) known for its ability to synthesize realistic images, leading to highly informative internal feature representations [90]. DINOv2 [70] is a self-supervised Vision Transformer that excels in capturing useful features through self-supervised contrastive learning. Combining these two models offers complementary strengths, which are rooted in their distinct learning paradigms [102]. While LDMs learn to generate images with a holistic understanding of the world, capturing both global and local information, DINO focuses on extracting meaningful features with invariance to spatial information, i.e. local position and global orientation, due to its input augmentations during training.

3.2. Framework

Multi-Teacher Distillation. Our method aims to distill information from two large vision foundation models

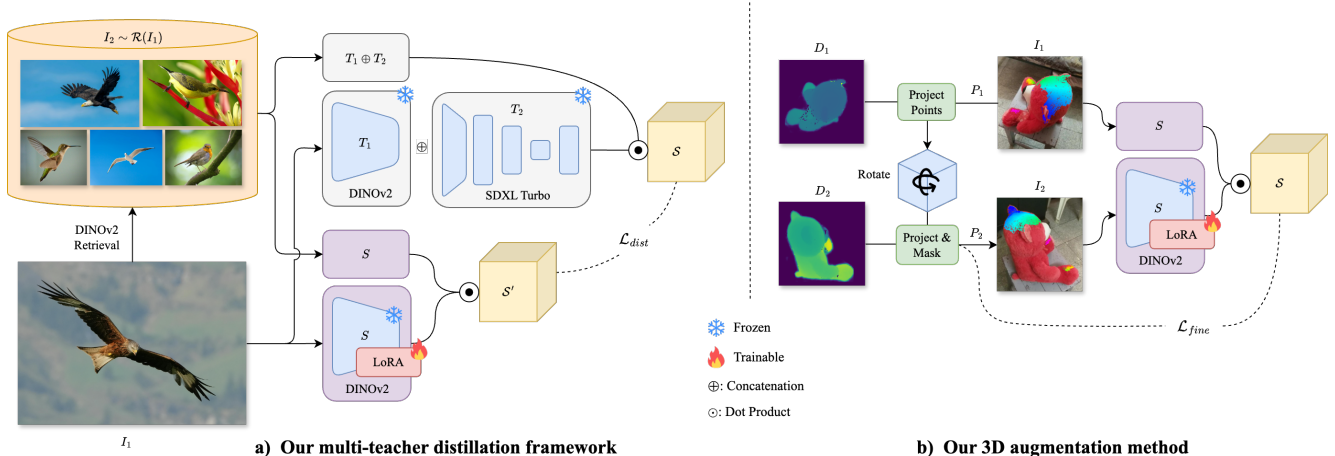


Figure 2. **Illustration of our multi-teacher distillation framework (a) and 3D data augmentation method (b).** We distill two complementary models, DINOv2 and SDXL Turbo, into one single and more efficient model. Using unsupervised 3D data augmentation we further refine our distilled model to achieve new state-of-the-art in both throughput and performance.

into a single student model that provides fast inference with accurate predictions. Therefore, we employ multi-teacher distillation with two teacher models T_1, T_2 and one student model S , where T_1 is a ViT and T_2 is a diffusion model. To achieve our goal of parameter-efficient training, we initialize the student model with a pre-trained vision model and incorporate Low-Rank Adaptation (LoRA) [35]. LoRA uses two smaller matrices, $A \in \mathbb{R}^{r \times k}$ and $B \in \mathbb{R}^{d \times r}$, whose dot product $\Delta W = BA$ matches the size of the model’s initial weight matrix $W \in \mathbb{R}^{d \times k}$, with its size controlled by $r \ll \min(d, k)$. Following [3, 16, 106], we apply LoRA only to the projection layers of the queries and values and keep all other parameters fixed:

$$\begin{aligned} Q &= W_Q x + B_Q A_Q x, \\ V &= W_V x + B_V A_V x, \\ K &= W_K x, \end{aligned} \quad (2)$$

where W_Q, W_K and W_V are the frozen projection layers and B_Q, A_Q and B_V, A_V are the trainable LoRA layers. The weights of B_Q and B_V are initialized with zeros. Besides parameter efficiency, this also mitigates the problem of catastrophic forgetting [7]. We utilize the predicted feature maps of an image pair to obtain the similarity maps of the teacher and student. The objective of the distillation is to align these similarity distributions. Thus, our approach is fully unsupervised by leveraging pseudo-labeling instead of human-annotated correspondences. Specifically, we pass an image I_1 to T_1 while we pass multiple noised versions $I_1 + \epsilon_t$ to T_2 . We average the extracted feature maps of T_2 and concatenate them with the extracted feature map of T_1 to form a combined feature map \mathcal{F}_1 . We input the same image I_1 to the student S and extract the feature map \mathcal{F}'_1 from it.

However, manually selected image pairs are scarce. To exclude any supervision while still having image pairs that are beneficial for the distillation, we propose to use image retrieval during training. The goal is to find a set of semantically similar images $\mathcal{R}(I_1)$ for a given image I_1 . After finding such a set, we sample and process a second image $I_2 \sim \mathcal{R}(I_1)$ in the same way as I_1 , to obtain feature maps \mathcal{F}_2 and \mathcal{F}'_2 .

We compute the cosine similarity of *all vectors* of the teacher feature maps $\mathcal{F}_1, \mathcal{F}_2$ and the student feature maps $\mathcal{F}'_1, \mathcal{F}'_2$ to obtain the similarity maps \mathcal{S} and \mathcal{S}' with shape $(H \times W) \times (H' \times W')$ using:

$$\text{sim}(\mathcal{F}_1, \mathcal{F}_2) = \mathcal{F}_1 \cdot \mathcal{F}_2^T = \mathcal{S} \quad (3)$$

We apply softmax with temperature $\sigma_\tau(\cdot)$ to ensure that each descriptor has a sharp but distributed similarity over all other descriptors. We use cross-entropy as a dense objective over all $(W \times H)^2$ correspondences simultaneously. Hence, we define the final training objective as:

$$\begin{aligned} \mathcal{L}_{dist} &= \text{CE}(\sigma_\tau(\mathcal{F}_1 \cdot \mathcal{F}'_1{}^T), \sigma_\tau(\mathcal{F}_2 \cdot \mathcal{F}'_2{}^T)) \\ &= \text{CE}(\mathcal{S}, \mathcal{S}') \end{aligned} \quad (4)$$

Here, cross-entropy loss CE is defined as $\text{CE}(P, T) = -\mathbb{E}_P[\log T]$ where H is the cross-entropy of the distribution T relative to a distribution P . As a result, the student learns the approximate goal of dense image similarity instead of directly imitating the teacher’s features and lowering the feature dimension.

3D Data Augmentation. Because large and diverse annotated datasets for semantic correspondence are scarce, we utilize a large multi-view image dataset with corresponding depth maps, namely CO3D [72], to further enhance

our distilled model in an unsupervised manner. Specifically, with two images of different viewing angles I_1, I_2 , their corresponding depth maps D_1, D_2 , and camera parameters K_1, K_2 , we project all points of I_1 from screen view s into world view w using D_1, K_1 and project them back into screen view using K_2 :

$$T = T_{s \rightarrow w}(K_1) \cdot T_{w \rightarrow s}(K_2),$$

$$\hat{p} = \begin{pmatrix} p_x \\ p_y \\ D_1(p_x, p_y) \end{pmatrix} \cdot T, \quad (5)$$

where $T_{i \rightarrow j}(\cdot)$ is the transformation from coordinate system i to j . Using the difference in z -axis of the projected depth \hat{D}_2 to D_2 , we exclude points that are not visible after the transformation:

$$M(x, y) = \begin{cases} 1 & \text{if } |D_2(x, y) - \hat{D}_2(x, y)| < \epsilon, \\ 0 & \text{otherwise} \end{cases} \quad (6)$$

where M is the mask of mutually visible pixels and ϵ is the threshold parameter. Thus, we obtain *locally-dense* correspondences to fine-tune our model without any human annotations. Following [53], we apply a $k \times k$ Gaussian kernel $g_k(\cdot)$ to the correspondence points, resulting in a $(N \times H \times W)$ sized correspondence map. Furthermore, we apply softmax with temperature to the predicted similarity map \mathcal{S} . This yields two distributions, where we utilize cross-entropy as the learning objective, which leads to the final fine-tuning loss:

$$\mathcal{L}_{fine} = \text{CE}(\sigma_\tau(\mathcal{F}_1 \cdot \mathcal{F}_2^T), g_k(G)) \quad (7)$$

4. Experiments

Datasets. To validate the performance of our approach, we follow previous works [32, 54, 62, 90, 102, 103] and evaluate on the following benchmark datasets. SPair-71k [66] consists of 70,958 annotated image pairs, each carefully selected to include a wide variety of changes in viewpoint, scale, occlusion level, and truncation. PF-WILLOW [30] consists of 100 different images and 900 image pairs from 5 categories. CUB-200-2011 [93] contains 11,788 bird images of 200 categories, with 15 distinct part locations each. COCO [57] is a large-scale object detection, segmentation, key-point detection, and captioning dataset and consists of 328,000 images from 80 categories. CO3D [72] is a large multi-view image dataset that includes camera parameters, depth maps and segmentation masks and consists of almost 19,000 videos from 50 COCO categories.

Evaluation. We use the Percentage of Correct Keypoints (PCK) to evaluate the performance of correspondence. In this metric, a predicted keypoint is considered to be correct if it lies within a radius of $\alpha \cdot \max(h, w)$. We measure two

variants of PCK: $\text{PCK}_{\alpha=0.1} \text{img}$ and $\text{PCK}_{\alpha=0.1} \text{bbox}$, where “img” indicates that h, w are the dimensions of the image, whereas “bbox” indicates that h, w are the dimensions of the object’s bounding box, included in the corresponding dataset.

Similar to [103], we apply soft-argmax on a pre-defined window around the predicted target point (window soft-argmax [8]) during inference. Following [103], we horizontally flip the source image and calculate the global similarity between the target image and both the original and flipped source images. We choose the image with higher similarity for predicting point correspondences with the target image (pose-align) to mitigate the problem of left-right ambiguity. This method uses point labels e.g. “left paw”, “right paw”, only available in SPair-71k to switch repetitive points after the flipping process, therefore we consider this method to be weakly supervised.

Implementation Details. We employ two teacher models T_1, T_2 , where T_1 is a Vision Transformer and T_2 is a Diffusion Model. We use specific variants of DINOv2 and Stable Diffusion, namely DINOv2 B/14 with registers for the first teacher T_1 and the student S , and SDXL Turbo for the second teacher T_2 . Using DINOv2 as a prior for the student greatly enhances the efficiency of our proposed method and reduces computational demands. We extract the features of S and T_1 from layer 11, while we extract the features of T_2 from layer 1. For the ensemble method, we average the feature maps of the diffusion teacher T_2 of multiple timesteps $t \in \{51, 101, 151, 201\}$. We set the rank for the LoRA of S to $r = 8$ and the softmax temperature to $\tau = 0.01$. To align the shapes of all feature maps, we set the size of the input images for T_1 and S to 434×434 , while for T_2 we set it to 980×980 . Both T_1 and T_2 output feature maps with a spatial resolution of 31×31 . This results in a combined feature map shape of $31 \times 31 \times (768 + 1280)$. The student predicts feature maps with shape $31 \times 31 \times 768$. For distillation, we use a dropout of 0.05 on the LoRA layers, AdamW optimizer with a weight decay of 0.05, an initial learning rate of 0.0001, a step learning rate scheduler and train for 40 epochs on a small subset (12,000 samples) of the COCO dataset. We use the top $k = 10$ closest samples in the image retrieval process. During the 3D data augmentation process, we use a Gaussian blur with kernel size $k = 7$ and a masking threshold of $\epsilon = 0.01$. During supervised fine-tuning however, a final linear head (2 layers) is added to the model and trained for 8 epochs, while iteratively increasing the dropout to 0.1. We use the normalized feature matrices $\mathcal{F}_1, \mathcal{F}_2$ to eliminate the division by their lengths (dot-product similarity).

Model	Input size	#Params	#img/sec	SPair-71k	PF-WILLOW	CUB-200
Unsupervised						
DINOv2	840 × 840	87M	<u>7.2</u>	59.5	67.4	85.9
↳ smaller resolution	434 × 434	87M	28.6	59.2	65.8	85.3
DIFT [90]	768 × 768	1B	1.5	57.7	<u>76.4</u>	74.3
DINOv2+SD1.5 [102]	960 × 960	1.1B	0.4	<u>64.0</u>	74.8	<u>86.3</u>
<i>Ours</i>	434 × 434	87M	28.6	65.1	77.4	89.4
Weakly-supervised						
DINOv2+SD+Sphere [63]	960 × 960	<u>1B</u>	0.5	67.3	-	-
DINOv2+SD+Pose-Align [†] [103]	960 × 960	<u>1B</u>	0.8	<u>69.6</u>	-	-
<i>Ours</i> +Pose-Align [†]	434 × 434	87M	14.3	70.6	-	-

Table 1. Comparison of total parameter count, throughput (images per second) on a single NVIDIA A100 80GB and performance on different datasets. Performances are measured in $PCK_{\text{bbox}}@0.1$ per point, averaged over all points for PF-WILLOW and CUB200, and averaged over classes for SPair-71k. [†]: Pose-align can only be applied to datasets that include keypoint-specific labels. The best performances are **bold**, while the second-best are underlined.

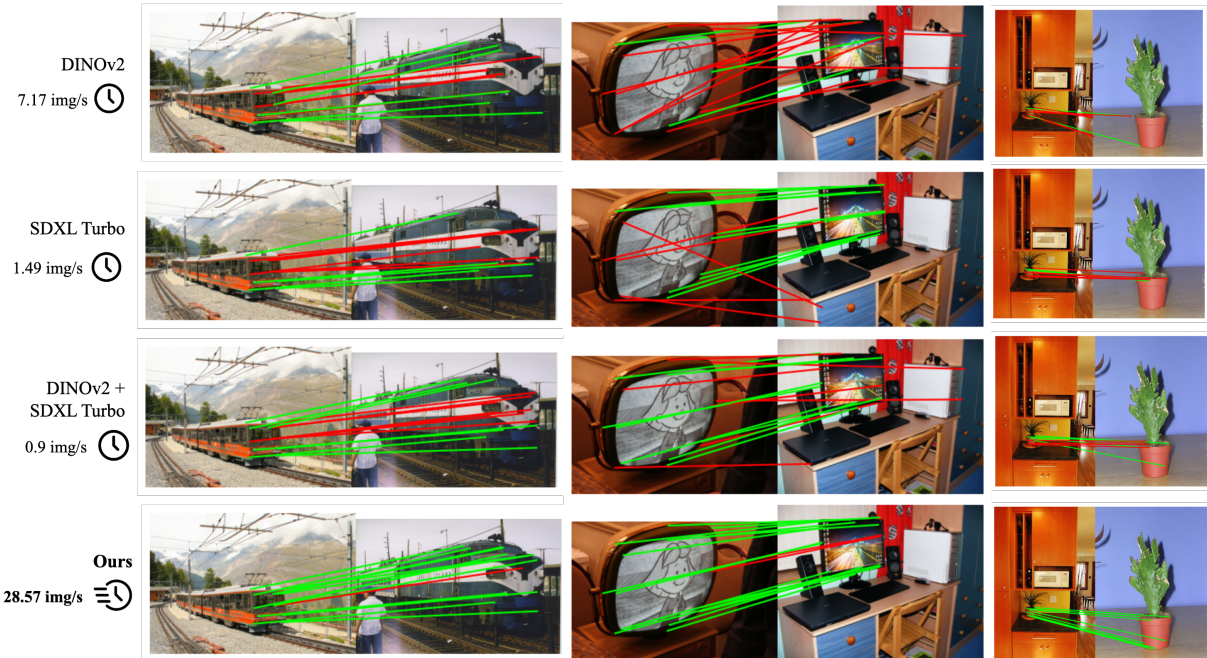


Figure 3. Examples image pairs from SPair-71k with predicted correspondences of different methods. Green indicates correct, while red indicates incorrect according to $PCK_{\text{bbox}}@0.1$. (840 × 840) was used as input resolution for DINOv2.

4.1. Comparison with State-of-the-Art

Tab. 1 and Fig. 3 show that our distilled model performs superior in both weakly-supervised and unsupervised correspondence compared to the current state-of-the-art. Notably, it achieves these results with far fewer parameters and thus far faster throughput compared to previous models, while drastically reducing computational load. This demonstrates that we can successfully distill information from two large vision foundation models into a smaller student model, without sacrificing performance. The model’s capa-

bility to work with smaller image sizes translates into fewer tokens processed, which additionally speeds up its performance. We were able to increase the number of images processed per second by a factor of 18, reduce the number of parameters by a factor of $\frac{1}{12}$ and improve $PCK_{\text{bbox}}@0.1$ by 0.6p compared to the current state-of-the-art in weakly-supervised semantic correspondence. The naive approach of concatenating the feature maps of both models, as how it was introduced in “A Tale of Two Features” [63, 102, 103], on the other hand, introduces significant overhead in terms

of VRAM and throughput, making the switch to our model an attractive option for real-time applications like semantic video correspondence, as seen in Fig. 4.

4.2. Ablations

Fine-Tuning Strategy. A common parameter-efficient fine-tuning strategy is to add a linear head at the end of the model. However, a linear head, applied to each token separately, may only capture local structures. Thus, we ablate two different fine-tuning strategies for distillation: Linear head (2 layers) and LoRA [35] (rank 8 on all layers). We exclude full fine-tuning, mainly to avoid catastrophic forgetting and the excessive training demands associated with it. As shown in Tab. 2, the linear layers are not sufficient for this distillation and our method with LoRA performs superior. Additionally, we ablate the rank parameter of LoRA, and our findings suggest that a low rank is sufficient for distillation while providing a good trade-off between performance and number of trainable parameters, see Fig. 5. In Tab. 5, we demonstrate that our 3D data augmentation method further improves the model, proving that semantic correspondence can be enhanced without any cost-intensive human keypoint annotations.

Point Sampling. Instead of aligning all point similarities within a feature map, only a subset of influential points could be used for distillation. We evaluate three different point sampling techniques: (1) sample pixels using source point annotations, (2) sample pixels that are mutual nearest neighbors, and (3) sample from all pixels within the image. Tab. 3 demonstrates, that the simplest approach of sampling all pixels leads to superior performance.

Image Sampling. Diverse pairs of images are crucial for effective distillation. However, SPair-71k only contains around 50 different images per category. Hence, we want to gradually shift to leveraging a large-scale dataset, instead of using manually selected image pairs provided by SPair-71k. We compare three alternative methods: (1) randomly combined images from the same category, (2) completely random combinations of images and (3) combining semantically similar images using retrieval. For the latter, we leverage DINOv2 embeddings to retrieve multiple similar target images for each source image. Tab. 4 shows that our proposed technique (retrieval pairs) achieves comparable results even without any supervision on an independent dataset (COCO).

Orthogonality to Previous Methods. In Tab. 5 we demonstrate, that current optimization techniques, such as an ensemble of varying diffusion timesteps $t \in 51, 101, 151, 201$ instead of a single timestep [90] during distillation, window soft-argmax, and pose-align [103],

Method	PCK _{bbox} @0.1	Trainable Params
Full Fine-tuning	62.12	86.88M
Linear Head	58.96	560K
LoRA	<u>61.77</u>	290K

Table 2. **Ablation of two different methods for parameter-efficient fine-tuning, evaluated on SPair-71k.** The best performances are **bold**, while the second-best are underlined.

Dataset	Method	PCK _{img} @0.1	PCK _{bbox} @0.1
SPair-71k	Source sampling	<u>69.92</u>	<u>60.22</u>
	Full sampling	71.67	62.37
COCO	Mutual-NN sampling	<u>70.35</u>	<u>61.24</u>
	Full sampling	71.06	62.02

Table 3. **Ablation of three different point sampling methods, trained on two different datasets and evaluated on SPair-71k.** Input resolutions for DINOv2 and SDXL Turbo are 434×434 and 980×980 respectively. The best performances are **bold**, while the second-best are underlined.

are also applicable to our model, further improving performance. Additionally, we apply our method to an independent dataset (COCO) to ensure minimal supervision and show that even in a completely unsupervised setting, our model is orthogonal to previous methods. Finally, we fine-tune our model to show its capabilities in a supervised setting and also compare it to the state-of-the-art in Tab. 6, demonstrating comparable performance at much higher throughput, highlighting the effectiveness of our method.

Other Downstream Tasks Our distillation and 3D augmentation protocol is tailored for (semantic) correspondence, but we also explore two downstream tasks: foreground segmentation with k-means and ImageNet-1k classification with k-NN probing. As shown in Fig. 6, our method qualitatively improves foreground segmentation and slightly outperforms DINOv2 on the DUTS saliency dataset (+0.01%). However, our model does not perform as well as DINOv2 on the ImageNet k-NN probing (-21.74%), suggesting that our model focuses more on local rather than global information.

5. Limitations

Despite these significant contributions, our method still has several limitations that need to be addressed in future work. One major limitation of our unsupervised model is the left-right ambiguity that arises when attempting to differentiate between symmetrical or repeated structures. This issue leads to inaccuracies in differentiating ambiguous parts, e.g. the left and right paws of a cat. Current works that try to address this issue, are all dependent on additional information either in the form of viewpoint information,



Figure 4. **Video semantic correspondence sample, showing accurate correspondences at a high frame rate.** We use source points on the first frame to calculate the corresponding points on all other frames at almost 30 FPS on an *NVIDIA A100 80GB*.

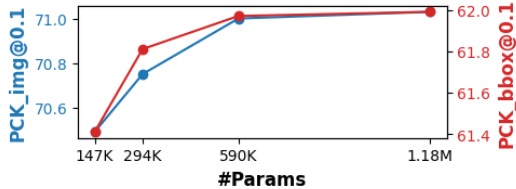


Figure 5. **Ablation of the rank parameter of LoRA, evaluated on SPair-71k.** Trained for 20 epochs on COCO with retrieval sampling. The #Params correspond to the ranks: 4, 8, 16 and 32, respectively.

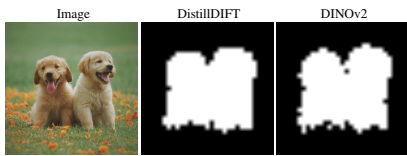


Figure 6. **Zero-shot foreground-background differentiation using k-means.** Our distilled model produces segmentation masks with less noisy edges.

Dataset	Method	PCK _{img} @0.1	PCK _{bbox} @0.1
SPair-71k	Manually selected pairs	71.67	62.37
	Random category pairs	70.11	60.76
	Random pairs	68.50	59.50
	Retrieval pairs	<u>70.61</u>	<u>61.59</u>
COCO	Random category pairs	<u>70.99</u>	<u>61.71</u>
	Retrieval pairs	71.06	62.02

Table 4. **Ablation of four different image sampling methods, trained on two different datasets and evaluated on SPair-71k.** Input resolutions for DINOv2 and SDXL Turbo are 434×434 and 980×980 respectively. The best performances are **bold**, while the second-best are underlined.

segmentation masks, or keypoint-specific labels [63, 103]. Another limitation of all current models is the handling of extreme deformations. For example, the legs of a cat can appear in highly varied positions and angles or even overlap, which can challenge the model’s ability to accurately correspond these parts across different images. Current state-of-the-art methods [63, 102, 103] still struggle with such deformations, and enhancing the model’s robustness to extreme deformations will be essential for improving its applicability to a wider range of real-world images.

Dataset	Method	PCK _{img} @0.1	PCK _{bbox} @0.1
SPair-71k	Full sampling	71.67	62.37
	+ Timestep ensemble	71.92	62.57
	+ Window soft-argmax	72.00	63.85
	+ Pose-align	<u>76.74</u>	<u>68.40</u>
	+ 3D (ours)	77.54	69.09
COCO	Retrieval pairs	71.06	62.02
	+ Window soft-argmax	72.36	63.35
	+ 3D (ours)	72.96	63.70

Table 5. **Ablation of different enhancement techniques applied to our method, trained on two different datasets and evaluated on SPair-71k.** The best performances are **bold**, while the second-best are underlined.

Method	#img/sec	PCK _{img} @0.1	PCK _{bbox} @0.1
[103] (w/o pre-train)	<u>0.4</u>	-	82.9
Retrieval pairs	28.6	71.06	62.02
+ Supervised fine-tuning		83.39	75.24
+ Window soft-argmax		84.73	77.06
+ Dropout		87.40	<u>80.19</u>

Table 6. **Ablation study on our supervised fine-tuning setting, trained and evaluated on SPair-71k.** The best performances are **bold**, while the second-best are underlined.

6. Conclusion

In summary, we successfully distill the knowledge from two large vision foundation models into a smaller student model to improve efficiency without sacrificing performance. Specifically, we leverage the complementary strengths of SDXL Turbo and DINOv2, to distill a more efficient model in terms of parameter count and throughput. Moreover, we introduce a novel unsupervised fine-tuning method that incorporates 3D data augmentation, enabling the model to achieve new state-of-the-art performance without the need for labeled data. Despite having fewer parameters and lower input image resolution, our approach demonstrates performance superior to state-of-the-art models across unsupervised, weakly-supervised, and supervised scenarios. This makes our distilled model suitable for resource-constrained environments and real-time applications, while also reducing computational demand during further training.

Acknowledgements

This project has been supported by the German Federal Ministry for Economic Affairs and Climate Action within the project “NXT GEN AI METHODS – Generative Methoden für Perzeption, Prädiktion und Planung”, the bid project KLIMA-MEMES, and the German Research Foundation (DFG) project 421703927. The authors gratefully acknowledge the Gauss Center for Supercomputing for providing compute through the NIC on JUWELS at JSC and the HPC resources supplied by the Erlangen National High Performance Computing Center (NHR@FAU funded by DFG).

References

- [1] Shir Amir, Yossi Gandelsman, Shai Bagon, and Tali Dekel. Deep vit features as dense visual descriptors. *CoRR*, abs/2112.05814, 2021. 1, 2
- [2] Tomer Amit, Tal Shaharabany, Eliya Nachmani, and Lior Wolf. Segdiff: Image segmentation with diffusion probabilistic models, 2022. 2
- [3] Reza Akbarian Bafghi, Nidhin Harilal, Claire Monteleoni, and Maziar Raissi. Parameter efficient fine-tuning of self-supervised vits without catastrophic forgetting, 2024. 4
- [4] Dmitry Baranchuk, Andrey Voynov, Ivan Rubachev, Valentin Khruikov, and Artem Babenko. Label-efficient semantic segmentation with diffusion models. In *The Tenth International Conference on Learning Representations, ICLR 2022, Virtual Event, April 25-29, 2022*. OpenReview.net, 2022. 2
- [5] Herbert Bay, Tinne Tuytelaars, and Luc Van Gool. Surf: Speeded up robust features. In Aleš Leonardis, Horst Bischof, and Axel Pinz, editors, *Computer Vision – ECCV 2006*, pages 404–417, Berlin, Heidelberg, 2006. Springer Berlin Heidelberg. 1, 2
- [6] Yoshua Bengio, Aaron C. Courville, and Pascal Vincent. Representation learning: A review and new perspectives. *IEEE Trans. Pattern Anal. Mach. Intell.*, 35(8):1798–1828, 2013. 3
- [7] Dan Biderman, Jose Javier Gonzalez Ortiz, Jacob Portes, Mansheej Paul, Philip Greengard, Connor Jennings, Daniel King, Sam Havens, Vitaliy Chiley, Jonathan Frankle, Cody Blakeney, and John P. Cunningham. Lora learns less and forgets less. *CoRR*, abs/2405.09673, 2024. 4
- [8] Adrian Bulat, Enrique Sanchez, and Georgios Tzimiropoulos. Subpixel heatmap regression for facial landmark localization. In *32nd British Machine Vision Conference 2021, BMVC 2021, Online, November 22-25, 2021*, page 422. BMVA Press, 2021. 5
- [9] Shoufa Chen, Peize Sun, Yibing Song, and Ping Luo. Diffusionet: Diffusion model for object detection. In *IEEE/CVF International Conference on Computer Vision, ICCV 2023*, pages 19773–19786. IEEE, 2023. 2
- [10] Ting Chen, Lala Li, Saurabh Saxena, Geoffrey E. Hinton, and David J. Fleet. A generalist framework for panoptic segmentation of images and videos. In *IEEE/CVF International Conference on Computer Vision, ICCV 2023*, pages 909–919. IEEE, 2023. 2
- [11] Seokju Cho, Sunghwan Hong, Sangryul Jeon, Yunsung Lee, Kwanghoon Sohn, and Seungryong Kim. Cats: Cost aggregation transformers for visual correspondence. In Marc’Aurelio Ranzato, Alina Beygelzimer, Yann N. Dauphin, Percy Liang, and Jennifer Wortman Vaughan, editors, *Advances in Neural Information Processing Systems 34*, pages 9011–9023, 2021. 1, 2
- [12] Seokju Cho, Sunghwan Hong, and Seungryong Kim. Cats++: Boosting cost aggregation with convolutions and transformers. *CoRR*, abs/2202.06817, 2022. 1, 2
- [13] Jooyoung Choi, Yunje Choi, Yunji Kim, Junho Kim, and Sungroh Yoon. Custom-edit: Text-guided image editing with customized diffusion models. *CoRR*, abs/2305.15779, 2023. 2
- [14] Christopher B. Choy, JunYoung Gwak, Silvio Savarese, and Manmohan Krishna Chandraker. Universal correspondence network. In Daniel D. Lee, Masashi Sugiyama, Ulrike von Luxburg, Isabelle Guyon, and Roman Garnett, editors, *Advances in Neural Information Processing Systems 29*, pages 2406–2414, 2016. 2
- [15] Guillaume Couairon, Jakob Verbeek, Holger Schwenk, and Matthieu Cord. Diffedit: Diffusion-based semantic image editing with mask guidance. In *The Eleventh International Conference on Learning Representations, ICLR 2023, Kigali, Rwanda, May 1-5, 2023*. OpenReview.net, 2023. 2
- [16] Beilei Cui, Mobarakol Islam, Long Bai, and Hongliang Ren. Surgical-dino: Adapter learning of foundation models for depth estimation in endoscopic surgery. *CoRR*, abs/2401.06013, 2024. 4
- [17] Prafulla Dhariwal and Alexander Quinn Nichol. Diffusion models beat gans on image synthesis. In Marc’Aurelio Ranzato, Alina Beygelzimer, Yann N. Dauphin, Percy Liang, and Jennifer Wortman Vaughan, editors, *Advances in Neural Information Processing Systems 34*, pages 8780–8794, 2021. 2
- [18] Alexey Dosovitskiy, Lucas Beyer, Alexander Kolesnikov, Dirk Weissenborn, Xiaohua Zhai, Thomas Unterthiner, Mostafa Dehghani, Matthias Minderer, Georg Heigold, Sylvain Gelly, Jakob Uszkoreit, and Neil Houlsby. An image is worth 16x16 words: Transformers for image recognition at scale. In *International Conference on Learning Representations*, 2021. 2
- [19] Yiqun Duan, Zheng Zhu, and Xianda Guo. Diffusiondepth: Diffusion denoising approach for monocular depth estimation. *CoRR*, abs/2303.05021, 2023. 2
- [20] Michael Fuest, Pingchuan Ma, Ming Gui, Johannes Schusterbauer, Vincent Tao Hu, and Bjorn Ommer. Diffusion models and representation learning: A survey. *arXiv preprint arXiv:2407.00783*, 2024. 2
- [21] Sanchit Gandhi, Patrick von Platen, and Alexander M. Rush. Distil-whisper: Robust knowledge distillation via large-scale pseudo labelling. *CoRR*, abs/2311.00430, 2023. 3
- [22] Shenyuan Gao, Chunlun Zhou, Chao Ma, Xinggang Wang, and Junsong Yuan. Aiatrack: Attention in attention

- for transformer visual tracking. In Shai Avidan, Gabriel J. Brostow, Moustapha Cissé, Giovanni Maria Farinella, and Tal Hassner, editors, *Computer Vision - ECCV 2022*, volume 13682 of *Lecture Notes in Computer Science*, pages 146–164. Springer, 2022. [1](#)
- [23] Abel Gonzalez-Garcia, Davide Modolo, and Vittorio Ferrari. Do semantic parts emerge in convolutional neural networks? *Int. J. Comput. Vis.*, 126(5):476–494, 2018. [2](#)
- [24] Ian J. Goodfellow, Jean Pouget-Abadie, Mehdi Mirza, Bing Xu, David Warde-Farley, Sherjil Ozair, Aaron C. Courville, and Yoshua Bengio. Generative adversarial networks. *CoRR*, abs/1406.2661, 2014. [2](#)
- [25] Jean-Bastien Grill, Florian Strub, Florent Altché, Corentin Tallec, Pierre Richemond, Elena Buchatskaya, Carl Doersch, Bernardo Avila Pires, Zhaohan Guo, Mohammad Gheshlaghi Azar, et al. Bootstrap your own latent—a new approach to self-supervised learning. *Advances in neural information processing systems*, 33:21271–21284, 2020. [2](#)
- [26] Jiatao Gu, Shuangfei Zhai, Yizhe Zhang, Lingjie Liu, and Josh M. Susskind. BOOT: data-free distillation of denoising diffusion models with bootstrapping. *CoRR*, abs/2306.05544, 2023. [3](#)
- [27] Yuxian Gu, Li Dong, Furu Wei, and Minlie Huang. Knowledge distillation of large language models. *CoRR*, abs/2306.08543, 2023. [3](#)
- [28] Ming Gui, Johannes Schusterbauer, Ulrich Prestel, Pingchuan Ma, Dmytro Kotovenko, Olga Grebenkova, Stefan Andreas Baumann, Vincent Tao Hu, and Björn Ommer. Depthfm: Fast monocular depth estimation with flow matching. *arXiv preprint arXiv:2403.13788*, 2024. [2](#)
- [29] Kamal Gupta, Varun Jampani, Carlos Esteves, Abhinav Shrivastava, Ameesh Makadia, Noah Snavely, and Abhishek Kar. ASIC: aligning sparse in-the-wild image collections. In *IEEE/CVF International Conference on Computer Vision, ICCV 2023*, pages 4111–4122. IEEE, 2023. [1](#), [2](#)
- [30] Bumsu Ham, Minsu Cho, Cordelia Schmid, and Jean Ponce. Proposal flow. In *2016 IEEE Conference on Computer Vision and Pattern Recognition, CVPR 2016, Las Vegas, NV, USA, June 27-30, 2016*, pages 3475–3484. IEEE Computer Society, 2016. [5](#)
- [31] Kai Han, Rafael S. Rezende, Bumsu Ham, Kwan-Yee K. Wong, Minsu Cho, Cordelia Schmid, and Jean Ponce. Snet: Learning semantic correspondence. In *IEEE International Conference on Computer Vision, ICCV 2017*, pages 1849–1858. IEEE Computer Society, 2017. [1](#)
- [32] Eric Hedlin, Gopal Sharma, Shweta Mahajan, Hosam Isack, Abhishek Kar, Andrea Tagliasacchi, and Kwang Moo Yi. Unsupervised semantic correspondence using stable diffusion. In Alice Oh, Tristan Naumann, Amir Globerson, Kate Saenko, Moritz Hardt, and Sergey Levine, editors, *Advances in Neural Information Processing Systems 36*, 2023. [1](#), [2](#), [5](#)
- [33] Amir Hertz, Ron Mokady, Jay Tenenbaum, Kfir Aberman, Yael Pritch, and Daniel Cohen-Or. Prompt-to-prompt image editing with cross-attention control. In *The Eleventh International Conference on Learning Representations, ICLR 2023, Kigali, Rwanda, May 1-5, 2023*. OpenReview.net, 2023. [2](#)
- [34] Geoffrey E. Hinton, Oriol Vinyals, and Jeffrey Dean. Distilling the knowledge in a neural network. *CoRR*, abs/1503.02531, 2015. [2](#), [3](#)
- [35] Edward J. Hu, Yelong Shen, Phillip Wallis, Zeyuan Allen-Zhu, Yuanzhi Li, Shean Wang, Lu Wang, and Weizhu Chen. Lora: Low-rank adaptation of large language models. In *The Tenth International Conference on Learning Representations, ICLR 2022, Virtual Event, April 25-29, 2022*. OpenReview.net, 2022. [4](#), [7](#)
- [36] Tao Hu, David W Zhang, Pascal Mettes, Meng Tang, Deli Zhao, and Cees G.M. Snoek. Latent space editing in transformer-based flow matching. In *AAAI*, 2024. [2](#)
- [37] Lin Huang, Tomas Hodan, Lingni Ma, Linguang Zhang, Luan Tran, Christopher D. Twigg, Po-Chen Wu, Junsong Yuan, Cem Keskin, and Robert Wang. Neural correspondence field for object pose estimation. In Shai Avidan, Gabriel J. Brostow, Moustapha Cissé, Giovanni Maria Farinella, and Tal Hassner, editors, *Computer Vision - ECCV 2022*, volume 13670 of *Lecture Notes in Computer Science*, pages 585–603. Springer, 2022. [1](#)
- [38] Allan Jabri, Andrew Owens, and Alexei A. Efros. Space-time correspondence as a contrastive random walk. In Hugo Larochelle, Marc’Aurelio Ranzato, Raia Hadsell, Maria-Florina Balcan, and Hsuan-Tien Lin, editors, *Advances in Neural Information Processing Systems 33*, 2020. [2](#)
- [39] Peng Jiang, Fanglin Gu, Yunhai Wang, Changhe Tu, and Baoquan Chen. Difnet: Semantic segmentation by diffusion networks. In Samy Bengio, Hanna M. Wallach, Hugo Larochelle, Kristen Grauman, Nicolò Cesa-Bianchi, and Roman Garnett, editors, *Advances in Neural Information Processing Systems 31*, pages 1637–1646, 2018. [2](#)
- [40] Wei Jiang, Eduard Trulls, Jan Hosang, Andrea Tagliasacchi, and Kwang Moo Yi. COTR: correspondence transformer for matching across images. In *2021 IEEE/CVF International Conference on Computer Vision, ICCV 2021*, pages 6187–6197. IEEE, 2021. [1](#), [2](#)
- [41] Bahjat Kawar, Shiran Zada, Oran Lang, Omer Tov, Huiwen Chang, Tali Dekel, Inbar Mosseri, and Michal Irani. Imagic: Text-based real image editing with diffusion models. In *IEEE/CVF Conference on Computer Vision and Pattern Recognition, CVPR 2023, Vancouver, BC, Canada, June 17-24, 2023*, pages 6007–6017. IEEE, 2023. [2](#)
- [42] Nikhil Varma Keetha, Avneesh Mishra, Jay Karhade, Krishna Murthy Jatavallabhula, Sebastian A. Scherer, K. Madhava Krishna, and Sourav Garg. Anyloc: Towards universal visual place recognition. *IEEE Robotics Autom. Lett.*, 9(2):1286–1293, 2024. [1](#)
- [43] Seungryong Kim, Stephen Lin, Sangryul Jeon, Dongbo Min, and Kwanghoon Sohn. Recurrent transformer networks for semantic correspondence. In Samy Bengio, Hanna M. Wallach, Hugo Larochelle, Kristen Grauman, Nicolò Cesa-Bianchi, and Roman Garnett, editors, *Advances in Neural Information Processing Systems 31*, pages 6129–6139, 2018. [1](#), [2](#)
- [44] Seungryong Kim, Dongbo Min, Bumsu Ham, Stephen Lin, and Kwanghoon Sohn. FCSS: fully convolutional self-similarity for dense semantic correspondence. *IEEE Trans. Pattern Anal. Mach. Intell.*, 41(3):581–595, 2019. [2](#)

- [45] Seungwook Kim, Juhong Min, and Minsu Cho. Transmatcher: Match-to-match attention for semantic correspondence. In *IEEE/CVF Conference on Computer Vision and Pattern Recognition, CVPR 2022, New Orleans, LA, USA, June 18-24, 2022*, pages 8687–8697. IEEE, 2022. 1, 2
- [46] Yoon Kim and Alexander M. Rush. Sequence-level knowledge distillation. In Jian Su, Xavier Carreras, and Kevin Duh, editors, *Proceedings of the 2016 Conference on Empirical Methods in Natural Language Processing, EMNLP 2016, Austin, Texas, USA, November 1-4, 2016*, pages 1317–1327. The Association for Computational Linguistics, 2016. 3
- [47] Filippos Kokkinos and Iasonas Kokkinos. To the point: Correspondence-driven monocular 3d category reconstruction. In Marc’Aurelio Ranzato, Alina Beygelzimer, Yann N. Dauphin, Percy Liang, and Jennifer Wortman Vaughan, editors, *Advances in Neural Information Processing Systems 34*, pages 7760–7772, 2021. 1
- [48] Junghyup Lee, Dohyung Kim, Jean Ponce, and Bumsuh Ham. Sfnet: Learning object-aware semantic correspondence. In *IEEE Conference on Computer Vision and Pattern Recognition, CVPR 2019, Long Beach, CA, USA, June 16-20, 2019*, pages 2278–2287. Computer Vision Foundation / IEEE, 2019. 2
- [49] Jae Yong Lee, Joseph DeGol, Victor Fragoso, and Sudipta N. Sinha. Patchmatch-based neighborhood consensus for semantic correspondence. In *IEEE Conference on Computer Vision and Pattern Recognition, CVPR 2021, virtual, June 19-25, 2021*, pages 13153–13163. Computer Vision Foundation / IEEE, 2021. 2
- [50] Alexander C. Li, Mihir Prabhudesai, Shivam Duggal, Ellis Brown, and Deepak Pathak. Your diffusion model is secretly a zero-shot classifier. In *IEEE/CVF International Conference on Computer Vision, ICCV 2023*, pages 2206–2217. IEEE, 2023. 2
- [51] Shuda Li, Kai Han, Theo W. Costain, Henry Howard-Jenkins, and Victor Prisacariu. Correspondence networks with adaptive neighbourhood consensus. In *2020 IEEE/CVF Conference on Computer Vision and Pattern Recognition, CVPR 2020, Seattle, WA, USA, June 13-19, 2020*, pages 10193–10202. Computer Vision Foundation / IEEE, 2020. 2
- [52] Xin Li, Deng-Ping Fan, Fan Yang, Ao Luo, Hong Cheng, and Zicheng Liu. Probabilistic model distillation for semantic correspondence. In *Proceedings of the IEEE/CVF Conference on Computer Vision and Pattern Recognition (CVPR)*, pages 7505–7514, June 2021. 3
- [53] Xinghui Li, Kai Han, Xingchen Wan, and Victor Adrian Prisacariu. Simsc: A simple framework for semantic correspondence with temperature learning. *CoRR*, abs/2305.02385, 2023. 5
- [54] Xinghui Li, Jingyi Lu, Kai Han, and Victor Prisacariu. Sd4match: Learning to prompt stable diffusion model for semantic matching. *CoRR*, abs/2310.17569, 2023. 2, 5
- [55] Yongqi Li and Wenjie Li. Data distillation for text classification. *arXiv preprint arXiv:2104.08448*, 2021. 2
- [56] Chuang Lin, Hongxun Yao, Wei Yu, and Xiaoshuai Sun. Cycle-consistency based hierarchical dense semantic correspondence. In *2018 IEEE International Conference on Image Processing, ICIP 2018, Athens, Greece, October 7-10, 2018*, pages 818–822. IEEE, 2018. 2
- [57] Tsung-Yi Lin, Michael Maire, Serge J. Belongie, Lubomir D. Bourdev, Ross B. Girshick, James Hays, Pietro Perona, Deva Ramanan, Piotr Dollár, and C. Lawrence Zitnick. Microsoft COCO: common objects in context. *CoRR*, abs/1405.0312, 2014. 5
- [58] Tony Lindeberg. *Scale Invariant Feature Transform*, volume 7. 05 2012. 1, 2
- [59] Ce Liu, Jenny Yuen, and Antonio Torralba. Sift flow: Dense correspondence across scenes and its applications. *IEEE Transactions on Pattern Analysis and Machine Intelligence*, 33(5):978–994, 2011. 2
- [60] Yifan Liu, Ke Chen, Chris Liu, Zengchang Qin, Zhenbo Luo, and Jingdong Wang. Structured knowledge distillation for semantic segmentation. In *Proceedings of the IEEE/CVF conference on computer vision and pattern recognition*, pages 2604–2613, 2019. 2
- [61] Jonathan Long, Ning Zhang, and Trevor Darrell. Do convnets learn correspondence? In Zoubin Ghahramani, Max Welling, Corinna Cortes, Neil D. Lawrence, and Kilian Q. Weinberger, editors, *Advances in Neural Information Processing Systems 27*, pages 1601–1609, 2014. 2
- [62] Grace Luo, Lisa Dunlap, Dong Huk Park, Aleksander Holynski, and Trevor Darrell. Diffusion hyperfeatures: Searching through time and space for semantic correspondence. In Alice Oh, Tristan Naumann, Amir Globerson, Kate Saenko, Moritz Hardt, and Sergey Levine, editors, *Advances in Neural Information Processing Systems 36*, 2023. 3, 5
- [63] Octave Mariotti, Oisín Mac Aodha, and Hakan Bilen. Improving semantic correspondence with viewpoint-guided spherical maps. *CoRR*, abs/2312.13216, 2023. 1, 3, 6, 8
- [64] Chenlin Meng, Robin Rombach, Ruiqi Gao, Diederik P. Kingma, Stefano Ermon, Jonathan Ho, and Tim Salimans. On distillation of guided diffusion models. In *IEEE/CVF Conference on Computer Vision and Pattern Recognition, CVPR 2023, Vancouver, BC, Canada, June 17-24, 2023*, pages 14297–14306. IEEE, 2023. 3
- [65] Zhong Meng, Jinyu Li, Yong Zhao, and Yifan Gong. Conditional teacher-student learning. In *IEEE International Conference on Acoustics, Speech and Signal Processing, ICASSP 2019, Brighton, United Kingdom, May 12-17, 2019*, pages 6445–6449. IEEE, 2019. 3
- [66] Juhong Min, Jongmin Lee, Jean Ponce, and Minsu Cho. Spair-71k: A large-scale benchmark for semantic correspondence. *CoRR*, abs/1908.10543, 2019. 5
- [67] Juhong Min, Jongmin Lee, Jean Ponce, and Minsu Cho. Learning to compose hypercolumns for visual correspondence. In Andrea Vedaldi, Horst Bischof, Thomas Brox, and Jan-Michael Frahm, editors, *Computer Vision - ECCV 2020*, volume 12360 of *Lecture Notes in Computer Science*, pages 346–363. Springer, 2020. 1
- [68] Jiteng Mu, Shalini De Mello, Zhiding Yu, Nuno Vasconcelos, Xiaolong Wang, Jan Kautz, and Sifei Liu. Coordgan: Self-supervised dense correspondences emerge from gans.

- In *IEEE/CVF Conference on Computer Vision and Pattern Recognition, CVPR 2022, New Orleans, LA, USA, June 18-24, 2022*, pages 10001–10010. IEEE, 2022. [2](#)
- [69] Soumik Mukhopadhyay, Matthew Gwilliam, Vatsal Agarwal, Namitha Padmanabhan, Archana Swaminathan, Srinidhi Hegde, Tianyi Zhou, and Abhinav Shrivastava. Diffusion models beat gans on image classification. *CoRR*, abs/2307.08702, 2023. [2](#)
- [70] Maxime Oquab, Timothée Darcet, Théo Moutakanni, Huy Vo, Marc Szafraniec, Vasil Khalidov, Pierre Fernandez, Daniel Haziza, Francisco Massa, Alaaeldin El-Nouby, Mahmoud Assran, Nicolas Ballas, Wojciech Galuba, Russell Howes, Po-Yao Huang, Shang-Wen Li, Ishan Misra, Michael G. Rabbat, Vasu Sharma, Gabriel Synnaeve, Hu Xu, Hervé Jégou, Julien Mairal, Patrick Labatut, Armand Joulin, and Piotr Bojanowski. Dinov2: Learning robust visual features without supervision. *CoRR*, abs/2304.07193, 2023. [3](#)
- [71] Seonguk Park and Nojun Kwak. FEED: feature-level ensemble for knowledge distillation. *CoRR*, abs/1909.10754, 2019. [3](#)
- [72] Jeremy Reizenstein, Roman Shapovalov, Philipp Henzler, Luca Sbordone, Patrick Labatut, and David Novotný. Common objects in 3d: Large-scale learning and evaluation of real-life 3d category reconstruction. In *2021 IEEE/CVF International Conference on Computer Vision, ICCV 2021*, pages 10881–10891. IEEE, 2021. [4](#), [5](#)
- [73] Ignacio Rocco, Relja Arandjelovic, and Josef Sivic. Convolutional neural network architecture for geometric matching. *IEEE Trans. Pattern Anal. Mach. Intell.*, 41(11):2553–2567, 2019. [1](#)
- [74] Ignacio Rocco, Relja Arandjelovic, and Josef Sivic. Efficient neighbourhood consensus networks via submanifold sparse convolutions. In Andrea Vedaldi, Horst Bischof, Thomas Brox, and Jan-Michael Frahm, editors, *Computer Vision - ECCV 2020*, volume 12354 of *Lecture Notes in Computer Science*, pages 605–621. Springer, 2020. [2](#)
- [75] Ignacio Rocco, Mircea Cimpoi, Relja Arandjelovic, Akihiko Torii, Tomás Pajdla, and Josef Sivic. Neighbourhood consensus networks. In Samy Bengio, Hanna M. Wallach, Hugo Larochelle, Kristen Grauman, Nicolò Cesa-Bianchi, and Roman Garnett, editors, *Advances in Neural Information Processing Systems 31*, pages 1658–1669, 2018. [2](#)
- [76] Robin Rombach, Andreas Blattmann, Dominik Lorenz, Patrick Esser, and Björn Ommer. High-resolution image synthesis with latent diffusion models. In *IEEE/CVF Conference on Computer Vision and Pattern Recognition, CVPR 2022, New Orleans, LA, USA, June 18-24, 2022*, pages 10674–10685. IEEE, 2022. [2](#), [3](#)
- [77] Adriana Romero, Nicolas Ballas, Samira Ebrahimi Kahou, Antoine Chassang, Carlo Gatta, and Yoshua Bengio. Fitnets: Hints for thin deep nets. In Yoshua Bengio and Yann LeCun, editors, *3rd International Conference on Learning Representations, ICLR 2015, San Diego, CA, USA, May 7-9, 2015, Conference Track Proceedings*, 2015. [3](#)
- [78] Tim Salimans and Jonathan Ho. Progressive distillation for fast sampling of diffusion models. In *The Tenth International Conference on Learning Representations, ICLR 2022, Virtual Event, April 25-29, 2022*. OpenReview.net, 2022. [2](#), [3](#)
- [79] Victor Sanh, Lysandre Debut, Julien Chaumond, and Thomas Wolf. Distilbert, a distilled version of BERT: smaller, faster, cheaper and lighter. *CoRR*, abs/1910.01108, 2019. [3](#)
- [80] Bharat Bhushan Sau and Vineeth N. Balasubramanian. Deep model compression: Distilling knowledge from noisy teachers. *CoRR*, abs/1610.09650, 2016. [3](#)
- [81] Saurabh Saxena, Abhishek Kar, Mohammad Norouzi, and David J. Fleet. Monocular depth estimation using diffusion models. *CoRR*, abs/2302.14816, 2023. [2](#)
- [82] Johannes Schusterbauer, Ming Gui, Pingchuan Ma, Nick Stracke, Stefan A. Baumann, Vincent Tao Hu, and Björn Ommer. Boosting latent diffusion with flow matching. In *ECCV*, 2024. [2](#)
- [83] Shuwei Shao, Zhongcai Pei, Weihai Chen, Dingchi Sun, Peter C. Y. Chen, and Zhengguo Li. Monodiffusion: Self-supervised monocular depth estimation using diffusion model. *CoRR*, abs/2311.07198, 2023. [2](#), [3](#)
- [84] Yujun Shi, Chuhui Xue, Jun Hao Liew, Jiachun Pan, Hanshu Yan, Wenqing Zhang, Vincent Y. F. Tan, and Song Bai. Dragdiffusion: Harnessing diffusion models for interactive point-based image editing, 2023. [2](#)
- [85] Ivan Shugurov, Sergey Zakharov, and Slobodan Ilic. Dpodv2: Dense correspondence-based 6 dof pose estimation. *IEEE Trans. Pattern Anal. Mach. Intell.*, 44(11):7417–7435, 2022. [1](#)
- [86] Yang Song, Prafulla Dhariwal, Mark Chen, and Ilya Sutskever. Consistency models. In Andreas Krause, Emma Brunskill, Kyunghyun Cho, Barbara Engelhardt, Sivan Sabato, and Jonathan Scarlett, editors, *International Conference on Machine Learning, ICML 2023*, volume 202 of *Proceedings of Machine Learning Research*, pages 32211–32252. PMLR, 2023. [3](#)
- [87] Mohammad Reza Taesiri, Giang Nguyen, and Anh Nguyen. Visual correspondence-based explanations improve AI robustness and human-ai team accuracy. In Sanmi Koyejo, S. Mohamed, A. Agarwal, Danielle Belgrave, K. Cho, and A. Oh, editors, *Advances in Neural Information Processing Systems 35*, 2022. [1](#)
- [88] Haoru Tan, Sitong Wu, and Jimin Pi. Semantic diffusion network for semantic segmentation. *CoRR*, abs/2302.02057, 2023. [2](#)
- [89] Weimin Tan, Siyuan Chen, and Bo Yan. Diffss: Diffusion model for few-shot semantic segmentation. *CoRR*, abs/2307.00773, 2023. [2](#)
- [90] Luming Tang, Menglin Jia, Qianqian Wang, Cheng Perng Phoo, and Bharath Hariharan. Emergent correspondence from image diffusion. In Alice Oh, Tristan Naumann, Amir Globerson, Kate Saenko, Moritz Hardt, and Sergey Levine, editors, *Advances in Neural Information Processing Systems 36*, 2023. [1](#), [3](#), [5](#), [6](#), [7](#)
- [91] Narek Tumanyan, Omer Bar-Tal, Shai Bagon, and Tali Dekel. Splicing vit features for semantic appearance transfer. In *IEEE/CVF Conference on Computer Vision and Pattern Recognition, CVPR 2022, New Orleans, LA, USA, June 18-24, 2022*, pages 10738–10747. IEEE, 2022. [1](#)

- [92] Narek Tumanyan, Michal Geyer, Shai Bagon, and Tali Dekel. Plug-and-play diffusion features for text-driven image-to-image translation. In *IEEE/CVF Conference on Computer Vision and Pattern Recognition, CVPR 2023, Vancouver, BC, Canada, June 17-24, 2023*, pages 1921–1930. IEEE, 2023. [2](#)
- [93] C. Wah, S. Branson, P. Welinder, P. Perona, and S. Belongie. Caltech-ucsd birds-200-2011 (cub-200-2011). Technical Report CNS-TR-2011-001, California Institute of Technology, 2011. [5](#)
- [94] Qianqian Wang, Xiaowei Zhou, Bharath Hariharan, and Noah Snavely. Learning feature descriptors using camera pose supervision. In Andrea Vedaldi, Horst Bischof, Thomas Brox, and Jan-Michael Frahm, editors, *Computer Vision - ECCV 2020*, volume 12346 of *Lecture Notes in Computer Science*, pages 757–774. Springer, 2020. [1](#), [2](#)
- [95] Xiaolong Wang, Allan Jabri, and Alexei A. Efros. Learning correspondence from the cycle-consistency of time. In *IEEE Conference on Computer Vision and Pattern Recognition, CVPR 2019, Long Beach, CA, USA, June 16-20, 2019*, pages 2566–2576. Computer Vision Foundation / IEEE, 2019. [1](#)
- [96] Julia Wolleb, Robin Sandkühler, Florentin Bieder, Philippe Valmaggia, and Philippe C. Cattin. Diffusion models for implicit image segmentation ensembles. In Ender Konukoglu, Bjoern H. Menze, Archana Venkataraman, Christian F. Baumgartner, Qi Dou, and Shadi Albarqouni, editors, *International Conference on Medical Imaging with Deep Learning, MIDL 2022, 6-8 July 2022, Zurich, Switzerland*, volume 172 of *Proceedings of Machine Learning Research*, pages 1336–1348. PMLR, 2022. [2](#)
- [97] Weijia Wu, Yuzhong Zhao, Mike Zheng Shou, Hong Zhou, and Chunhua Shen. Diffumask: Synthesizing images with pixel-level annotations for semantic segmentation using diffusion models. In *IEEE/CVF International Conference on Computer Vision, ICCV 2023*, pages 1206–1217. IEEE, 2023. [2](#)
- [98] Jiarui Xu, Sifei Liu, Arash Vahdat, Wonmin Byeon, Xiaolong Wang, and Shalini De Mello. Open-vocabulary panoptic segmentation with text-to-image diffusion models. In *IEEE/CVF Conference on Computer Vision and Pattern Recognition, CVPR 2023, Vancouver, BC, Canada, June 17-24, 2023*, pages 2955–2966. IEEE, 2023. [2](#)
- [99] Junho Yim, Donggyu Joo, Ji-Hoon Bae, and Junmo Kim. A gift from knowledge distillation: Fast optimization, network minimization and transfer learning. In *2017 IEEE Conference on Computer Vision and Pattern Recognition, CVPR 2017, Honolulu, HI, USA, July 21-26, 2017*, pages 7130–7138. IEEE Computer Society, 2017. [3](#)
- [100] Sergey Zagoruyko and Nikos Komodakis. Paying more attention to attention: Improving the performance of convolutional neural networks via attention transfer. In *5th International Conference on Learning Representations, ICLR 2017, Toulon, France, April 24-26, 2017, Conference Track Proceedings*. OpenReview.net, 2017. [3](#)
- [101] Matthew D. Zeiler and Rob Fergus. Visualizing and understanding convolutional networks. In David J. Fleet, Tomás Pajdla, Bernt Schiele, and Tinne Tuytelaars, editors, *Computer Vision - ECCV 2014*, volume 8689 of *Lecture Notes in Computer Science*, pages 818–833. Springer, 2014. [1](#), [2](#)
- [102] Junyi Zhang, Charles Herrmann, Junhwa Hur, Luisa Polania Cabrera, Varun Jampani, Deqing Sun, and Ming-Hsuan Yang. A tale of two features: Stable diffusion complements DINO for zero-shot semantic correspondence. In Alice Oh, Tristan Naumann, Amir Globerson, Kate Saenko, Moritz Hardt, and Sergey Levine, editors, *Advances in Neural Information Processing Systems 36*, 2023. [1](#), [2](#), [3](#), [5](#), [6](#), [8](#)
- [103] Junyi Zhang, Charles Herrmann, Junhwa Hur, Eric Chen, Varun Jampani, Deqing Sun, and Ming-Hsuan Yang. Telling left from right: Identifying geometry-aware semantic correspondence. *CoRR*, abs/2311.17034, 2023. [1](#), [3](#), [5](#), [6](#), [7](#), [8](#)
- [104] Wenliang Zhao, Yongming Rao, Zuyan Liu, Benlin Liu, Jie Zhou, and Jiwen Lu. Unleashing text-to-image diffusion models for visual perception. In *IEEE/CVF International Conference on Computer Vision, ICCV 2023*, pages 5706–5716. IEEE, 2023. [2](#)
- [105] Bolei Zhou, Aditya Khosla, Àgata Lapedriza, Aude Oliva, and Antonio Torralba. Learning deep features for discriminative localization. In *2016 IEEE Conference on Computer Vision and Pattern Recognition, CVPR 2016, Las Vegas, NV, USA, June 27-30, 2016*, pages 2921–2929. IEEE Computer Society, 2016. [2](#)
- [106] Yitao Zhu, Zhenrong Shen, Zihao Zhao, Sheng Wang, Xin Wang, Xiangyu Zhao, Dinggang Shen, and Qian Wang. Melo: Low-rank adaptation is better than fine-tuning for medical image diagnosis. *CoRR*, abs/2311.08236, 2023. [4](#)

Appendix

A. Softmax Temperature Ablation

In Fig. 7, we ablate different values for τ for $\sigma_\tau(\cdot)$. Higher values result in smoother distributions, while lower values result in sharper distributions. We show that the sweet-spot for this parameter is at 0.01.

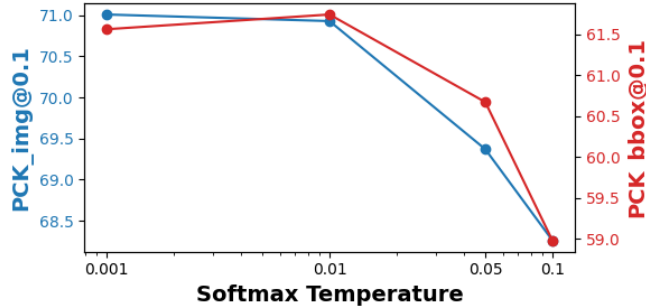


Figure 7. Ablation of the softmax temperature parameter τ , evaluated on SPair-71k. Trained for 10 epochs on COCO with retrieval sampling.

B. 3D Threshold Ablation

Fig. 8 shows the effect of the threshold parameter ϵ on our 3D data augmentation method. Smaller values tend to exclude more points that are on the visible surface, whereas larger values tend to include too many points that are not on the visible surface. We set this parameter to 0.01 as it shows a good balance between those to extremes.

C. Model Analysis

In Tab. 7 and Tab. 8 we ablate different Diffusion- and ViT-based models to find the best combination. We show that SDXL Turbo and DINOv2 (vitb14) with registers are the best performing models in our evaluation. In Tab. 9 we ablate different combinations of models to find the best performing setting. We show that the combination of the best performing models in the individual ablation, are also the best performing combination in general. Increasing the input resolution and adding additional layers further boosts the performance. In Table 10 we ablate the use of an additional strong teacher model, namely CLIP. However, we did not find any improvement in adding this model to the teacher ensemble.

Model	SPair-71K	PF-WILLOW	CUB-200	S	T	L
SD1.5	66.11/56.24	86.58/73.60	90.58/79.18	768 ²	201	5
SD2.1	65.29/57.87	87.18/74.83	88.63/78.23	768 ²	261	8
SDXL Base	64.02/55.52	<u>88.37/76.49</u>	92.39/84.20	768 ²	101	1
SDXL Base	65.64/57.87	88.58/76.30	92.41/84.20	1024 ²	201	1
LCM-XL	62.9/54.5	86.52/73.81	92.59/84.40	768 ²	64	1
SDXL Turbo	<u>67.26/58.54</u>	89.59/77.76	<u>93.54/85.57</u>	768 ²	101	1
SDXL Turbo	67.40/59.50	88.48/76.44	93.35/85.72	1024 ²	101	1

Table 7. The performance of different diffusion-based models evaluated on different datasets. Values are measured in PCK@0.1 (img/bbox), per keypoint and averaged over all keypoints. S: Size of the input image, T: Timestep, L: Layer. Prompt for all models: “a photo of a [category]”.

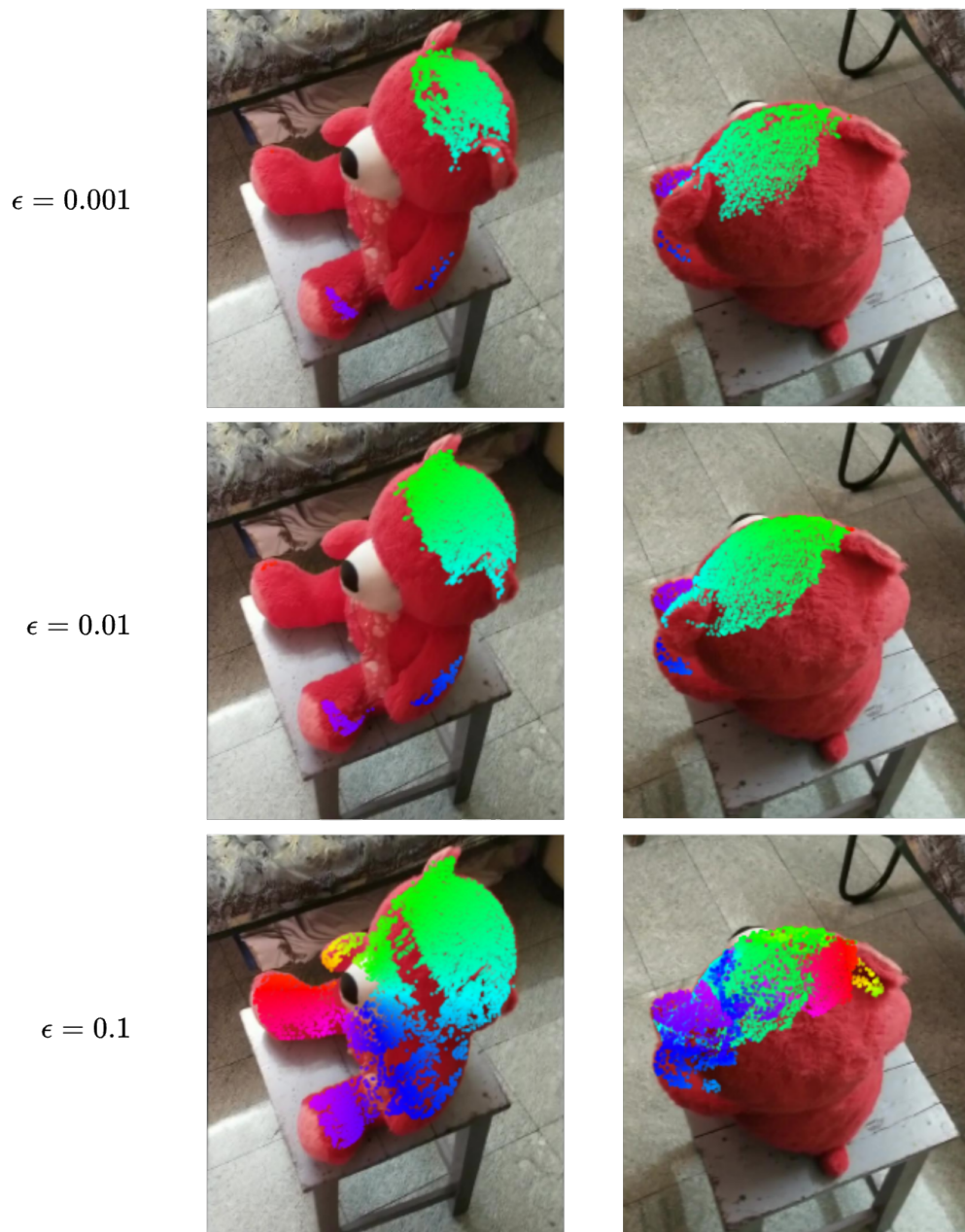


Figure 8. The effect of the 3D data threshold parameter ϵ .

Method	$\text{PCK}_{\text{img}}@0.1$	$\text{PCK}_{\text{bbox}}@0.1$
DINOv2 + SD	71.77	63.29
DINOv2 + SD + CLIP	<u>68.87</u>	<u>60.17</u>

Table 10. Performance on SPair-71k for different teachers. Adding CLIP to the teacher ensemble does not improve performance.

Model	SPair-71K	PF-WILLOW	CUB-200	R	L
CLIP _(ViT-L-14)	47.05/37.05	73.51/57.67	82.31/67.86	336 ²	11
MAE _(ViT-L-14)	33.26/23.99	73.04/56.54	64.25/45.04	224 ²	26
ZoeDepth	12.80/6.63	38.47/25.93	22.90/9.75	512 × 384	10 (BeiT)
I-JEPA _(ViT-H-16-448)	51.88/44.78	—/—	—/—	448 ²	31
DINOv1 _(ViT-S-8)	46.69/35.92	61.66/47.99	84.06/70.09	224 ²	9
DINOv2 _(ViT-B-14)	<u>67.45/57.69</u>	84.14/68.78	<u>94.54/85.90</u>	840 ²	11
DINOv2R _(ViT-B-14)	69.10/58.83	<u>83.07/67.38</u>	94.61/85.90	840 ²	11

Table 8. **The performance of different ViT-based models evaluated on different datasets.** Values are measured in PCK@0.1 (img/bbox), per keypoint and averaged over all keypoints. S: Size of the input image, L: Layer.

Model	SPair-71K	PF-WILLOW	CUB-200	S	T	L
SD1.5 + DINOv2	71.57/62.03	89.02/75.94	94.43/85.27	840 ²	201	5 + 11
SD1.5 + DINOv2	71.38/62.08	88.84/75.70	94.24/85.69	840 ²	201	3, 7, 11 + 11
SD1.5 + DINOv2	<u>71.67/63.08</u>	88.43/74.84	94.55/86.25	960 ²	100	3, 7, 11 + 11
SDXL Turbo + DINOv2	70.90/61.88	89.77/76.62	<u>94.89/86.45</u>	840 ²	101	1 + 11
SDXL Turbo + DINOv2	71.21/62.79	88.03/74.76	94.22/85.81	840 ²	101	1, 4, 7 + 11
SDXL Turbo + DINOv2	71.77/63.29	<u>89.36/75.98</u>	94.83/87.43	980 ²	101	1 + 11

Table 9. **The performance of different combinations of models and layers evaluated on different datasets.** Values are measured in PCK@0.1 (img/bbox), per keypoint and averaged over all keypoints. With DINOv2, we mean DINOv2 (ViT-B-14) with registers. S: Size of the input image, T: Timestep, L: Layer. Prompt for all models: “a photo of a [category]”.

D. Foreground Segmentation

We assess our model on other downstream tasks, including zero-shot foreground/ background segmentation. The examples in Figure 9 show a marginal improvement in mask quality. The masks generated with our model are slightly less noisy compared to the baseline DINOv2 model.

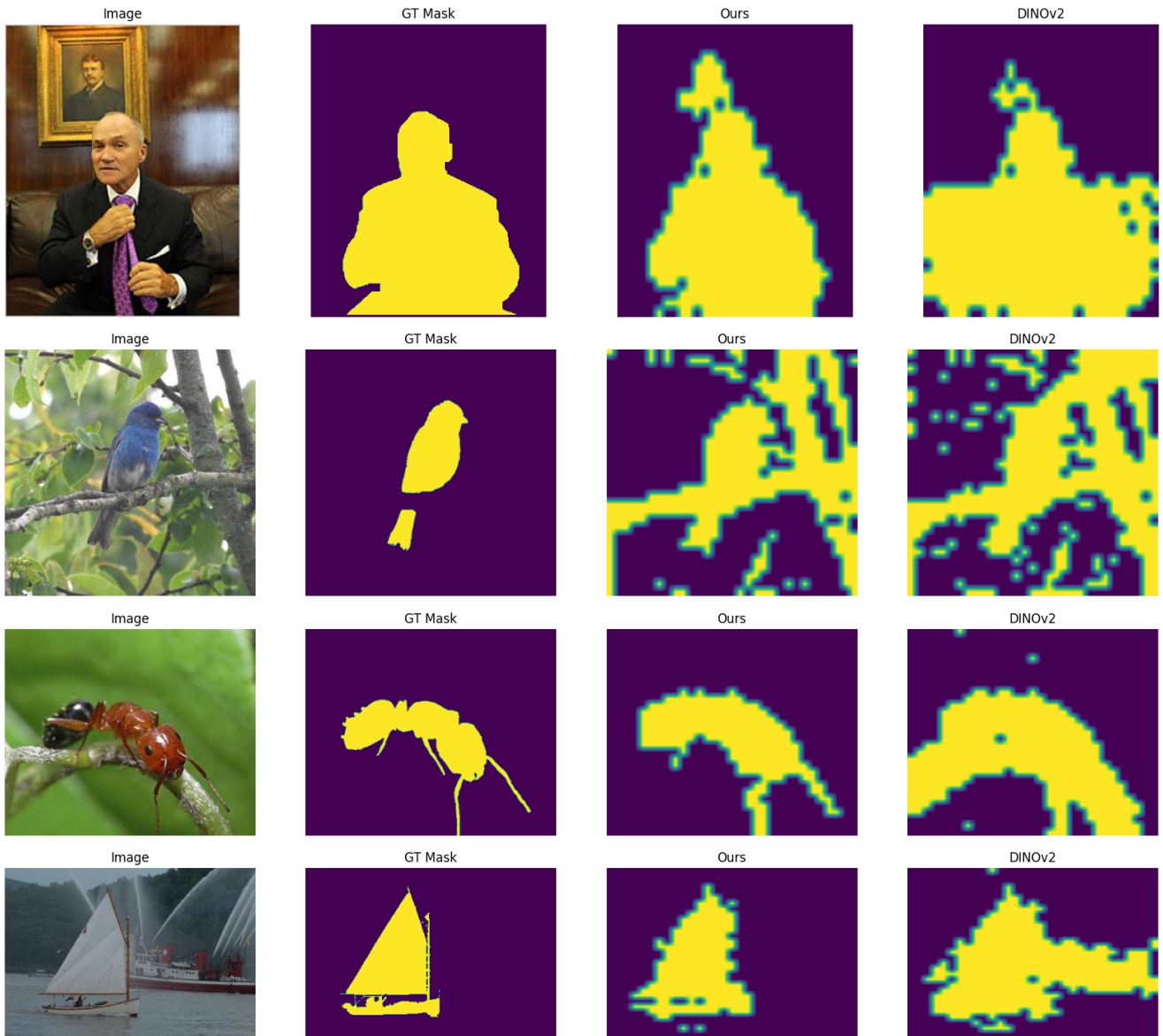


Figure 9. Examples of the improved foreground/background segmentation masks with our model.

Supplementary Material

0.1 Softmax Temperature Ablation

In Fig. 1, we ablate different values for τ for $\sigma_\tau(\cdot)$. Higher values result in smoother distributions, while lower values result in sharper distributions. We show that the sweet-spot for this parameter is at 0.01.

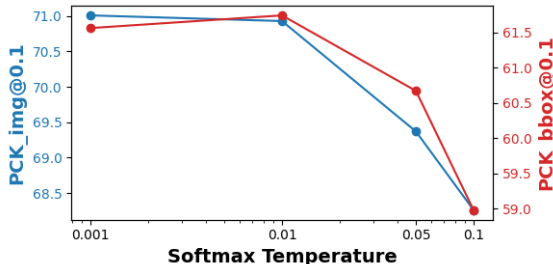


Figure 1: Ablation of the softmax temperature parameter τ , evaluated on SPair-71k. Trained for 10 epochs on COCO with retrieval sampling.

0.2 3D Threshold Ablation

Fig. 2 shows the effect of the threshold parameter ϵ on our 3D data augmentation method. Smaller values tend to exclude more points that are on the visible surface, whereas larger values tend to include too many points that are not on the visible surface. We set this parameter to 0.01 as it shows a good balance between those to extremes.

0.3 Model Analysis

In Tab. 1 and Tab. 2 we ablate different Diffusion- and ViT-based models to find the best combination. We show that SDXL Turbo and DINOv2 (vitb14) with registers are the best performing models in our evaluation. In Tab. 3 we ablate different combinations of models to find the best performing setting. We show that the combination of the best performing models in the individual ablation, are also the best performing combination in general. Increasing the input resolution and adding additional layers further boosts the performance. In Table 4 we ablate the use of an additional strong teacher model, namely CLIP. However, we did not find any improvement in adding this model to the teacher ensemble.

Method	PCK _{img} @0.1	PCK _{bbox} @0.1
DINOv2 + SD	71.77	63.29
DINOv2 + SD + CLIP	<u>68.87</u>	<u>60.17</u>

Table 4: Performance on SPair-71k for different teachers. Adding CLIP to the teacher ensemble does not improve performance.

0.4 Foreground Segmentation

We assess our model on other downstream tasks, including zero-shot foreground/ background segmentation. The examples in Figure 3 show a marginal improvement in mask quality. The masks generated with our model are slightly less noisy compared to the baseline DINOv2 model.

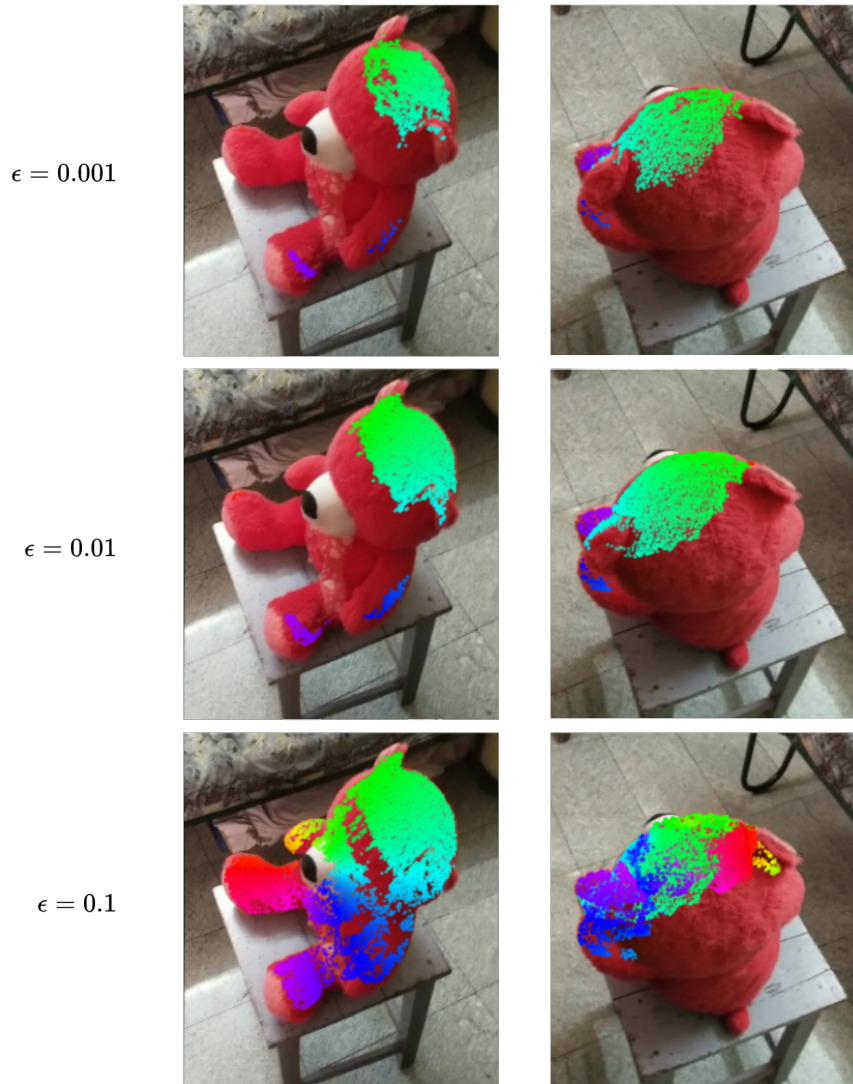


Figure 2: The effect of the 3D data threshold parameter ϵ .

Model	SPair-71K	PF-WILLOW	CUB-200	S	T	L
SD1.5	66.11/56.24	86.58/73.60	90.58/79.18	768 ²	201	5
SD2.1	65.29/57.87	87.18/74.83	88.63/78.23	768 ²	261	8
SDXL Base	64.02/55.52	<u>88.37/76.49</u>	92.39/84.20	768 ²	101	1
SDXL Base	65.64/57.87	88.58/76.30	92.41/84.20	1024 ²	201	1
LCM-XL	62.9/54.5	86.52/73.81	92.59/84.40	768 ²	64	1
SDXL Turbo	<u>67.26/58.54</u>	89.59/77.76	<u>93.54/85.57</u>	768 ²	101	1
SDXL Turbo	67.40/59.50	88.48/76.44	93.35/85.72	1024 ²	101	1

Table 1: The performance of different diffusion-based models evaluated on different datasets. Values are measured in PCK@0.1 (img/bbox), per keypoint and averaged over all keypoints. S: Size of the input image, T: Timestep, L: Layer. Prompt for all models: “a photo of a [category]”.

Model	SPair-71K	PF-WILLOW	CUB-200	R	L
CLIP (ViT-L-14)	47.05/37.05	73.51/57.67	82.31/67.86	336 ²	11
MAE (ViT-L-14)	33.26/23.99	73.04/56.54	64.25/45.04	224 ²	26
ZoeDepth	12.80/6.63	38.47/25.93	22.90/9.75	512 × 384	10 (BeiT)
I-JEPA (ViT-H-16 448)	51.88/44.78	—/—	—/—	448 ²	31
DINOv1 (ViT-S-8)	46.69/35.92	61.66/47.99	84.06/70.09	224 ²	9
DINOv2 (ViT-B-14)	67.45/57.69	84.14/68.78	<u>94.54/85.90</u>	840 ²	11
DINOv2R (ViT-B-14)	69.10/58.83	<u>83.07/67.38</u>	94.61/85.90	840 ²	11

Table 2: **The performance of different ViT-based models evaluated on different datasets.** Values are measured in PCK@0.1 (img/ bbox), per keypoint and averaged over all keypoints. S: Size of the input image, L: Layer.

Model	SPair-71K	PF-WILLOW	CUB-200	S	T	L
SD1.5 + DINOv2	71.57/62.03	89.02/75.94	94.43/85.27	840 ²	201	5 + 11
SD1.5 + DINOv2	71.38/62.08	88.84/75.70	94.24/85.69	840 ²	201	3, 7, 11 + 11
SD1.5 + DINOv2	<u>71.67/63.08</u>	88.43/74.84	94.55/86.25	960 ²	100	3, 7, 11 + 11
SDXL Turbo + DINOv2	70.90/61.88	89.77/76.62	<u>94.89/86.45</u>	840 ²	101	1 + 11
SDXL Turbo + DINOv2	71.21/62.79	88.03/74.76	94.22/85.81	840 ²	101	1, 4, 7 + 11
SDXL Turbo + DINOv2	71.77/63.29	<u>89.36/75.98</u>	94.83/87.43	980 ²	101	1 + 11

Table 3: **The performance of different combinations of models and layers evaluated on different datasets.** Values are measured in PCK@0.1 (img/ bbox), per keypoint and averaged over all keypoints. With DINOv2, we mean DINOv2 (ViT-B-14) with registers. S: Size of the input image, T: Timestep, L: Layer. Prompt for all models: “a photo of a [category]”.

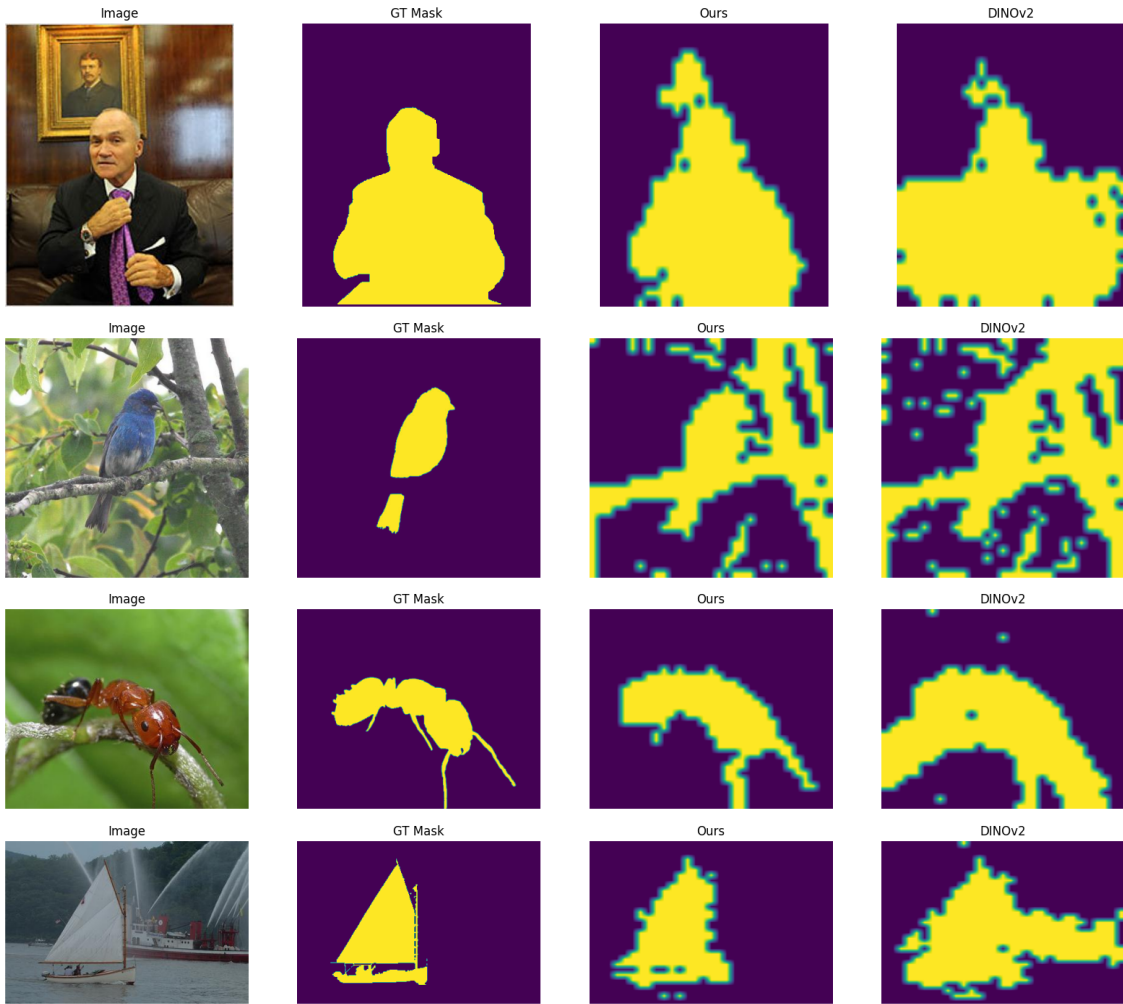


Figure 3: Examples of the improved foreground/background segmentation masks with our model.